Theoretical study of solvent effects on the coil-globule transition

James M. Polson,[a] Sheldon B. Opps, and Nicholas Abou Risk
Department of Physics, University of Prince Edward Island, 550 University Ave., Charlottetown, Prince Edward Island C1A 4P3, Canada

(Received 6 February 2009; accepted 21 May 2009; published online 24 June 2009)

The coil-globule transition of a polymer in a solvent has been studied using Monte Carlo simulations of a single chain subject to intramolecular interactions as well as a solvent-mediated effective potential. This solvation potential was calculated using several different theoretical approaches for two simple polymer/solvent models, each employing hard-sphere chains and hard-sphere solvent particles as well as attractive square-well potentials between some interaction sites. For each model, collapse is driven by variation in a parameter which changes the energy mismatch between monomers and solvent particles. The solvation potentials were calculated using two fundamentally different methodologies, each designed to predict the conformational behavior of polymers in solution: (1) the polymer reference interaction site model (PRISM) theory and (2) a many-body solvation potential (MBSP) based on scaled particle theory introduced by Grayce [J. Chem. Phys. **106**, 5171 (1997)]. For the PRISM calculations, two well-studied solvation monomer-monomer pair potentials were employed, each distinguished by the closure relation used in its derivation: (i) a hypernetted-chain (HNC)-type potential and (ii) a Percus–Yevick (PY)-type potential. The theoretical predictions were each compared to results obtained from explicit-solvent discontinuous molecular dynamics simulations on the same polymer/solvent model systems [J. Chem. Phys. **125**, 194904 (2006)]. In each case, the variation in the coil-globule transition properties with solvent density is mostly qualitatively correct, though the quantitative agreement between the theory and prediction is typically poor. The HNC-type potential yields results that are more qualitatively consistent with simulation. The conformational behavior of the polymer upon collapse predicted by the MBSP approach is quantitatively correct for low and moderate solvent densities but is increasingly less accurate for higher densities. At high solvent densities, the PRISM-HNC and MBSP approaches tend to overestimate, while the PRISM-PY approach underestimates the tendency of the solvent to drive polymer collapse. © *2009 American Institute of Physics*.
[DOI: 10.1063/1.3153350]

I. INTRODUCTION

The conformational properties of polymers in solution are governed by the complex set of interactions among the polymer and solvent molecules as well as the thermodynamic conditions of the solution. A noteworthy illustration of this relationship is the polymer collapse transition, a phenomenon in which individual polymers in dilute solution undergo a significant reduction in their average size upon a change in the solvent conditions. In the so-called "good" solvent conditions, the polymer exists in the coil state, which is characterized by open or expanded conformation and maximal polymer/solvent contact, while in "poor" solvent conditions, the polymer assumes a compact liquidlike structure characterized by minimal polymer/solvent contact. Between these two states lies the so-called "theta" point, at which the polymer assumes many of the conformational properties of an ideal chain. The solvent conditions that determine these conformational states can be tuned in a variety of ways, including variations in the temperature, *p*H, or chemical composition of the solvent. Since its first experimental observation,[1,2] the coil-globule transition has been the subject of intense experimental and theoretical inquiry in part due to its similarity to protein folding, as well as its relevance to the stability of polymer solutions. Several years ago, Baysal and Karasz published a comprehensive review of much of this work.[3]

A thorough theoretical treatment of the polymer collapse transition clearly requires a methodology to study the solvent effects on the conformational behavior of the polymer chain. Many approaches to this problem have borrowed techniques from liquid state theory and extended them to polymer solutions. For example, Gan and Eu developed an integral equation theory based on the Kirkwood equation and applied it to study model polymers in good and poor solvents and for athermal polymer/solvent systems.[4] Taylor and Lipson used the Born–Green–Yvon equation to study solvent effects of a single polymer in a solvent.[5] Taylor later developed a theoretical density expansion of the set of intramolecular distribution functions and applied it to an athermal system of a single polymer in a solvent for various polymer/solvent size ratios for short chains.[6] More recently, Taylor *et al.* developed a theoretical approach to study the conformational behavior of polymer chains using a pairwise-additive solvation potential using intrachain correlation functions obtained from explicit-solvent Monte Carlo (MC) simulations of

[a]Electronic mail: jpolson@upei.ca.

5-mers.[7,8] Other theoretical approaches to studying solvent effects on polymers in solution include density functional theory[9] and Flory–Huggins mean-field theory.[10]

The polymer reference interaction site model (PRISM) theory developed by Curro and Schweizer[11–13] offers another theoretical approach for studying conformational properties of polymeric systems. An extension of the reference interaction site model (RISM) theory[14,15] of molecular fluids, PRISM theory uses integral equation methods to calculate intermolecular site-site correlation functions for flexible chain molecules. The PRISM equation is essentially a generalized Ornstein–Zernicke equation whose solution requires appropriate closure relations. A complicating feature of the PRISM equation is its dependence on the static structure factor of the polymer chain, a quantity that is not known *a priori*. One means to calculate the structure factor is to perform a MC simulation of an isolated chain molecule. However, since the medium surrounding a flexible polymer influences its conformational behavior, the effects of the medium must be built into the MC simulation model. This can be achieved using a suitably chosen solvation potential. For simplicity, the solvation potential is often assumed to be pairwise additive in form. In addition, the solvation potentials commonly employed in such calculations usually depend on the intermolecular site-site correlation functions. Consequently, the PRISM equations need to be solved self-consistently with the MC simulation. The expressions for solvation pair potentials can be derived using the RISM equations together with appropriate closure relations. The first potential derived in this manner used the hypernetted-chain (HNC) approximation.[16] Subsequently, Grayce and co-workers derived a different relation using the Percus–Yevick (PY) closure relation.[17,18] Other solvation pair potentials have been proposed, but the HNC-type potential has been employed most widely.

Application of the self-consistent hybrid MC/PRISM method to study the conformational properties of a single chain in a solvent was first carried out by Khokhlov and co-workers.[19–21] They studied the static properties of repulsive Lennard-Jones chains in a monomeric solvent and found them to be quantitatively consistent with explicit-solvent molecular dynamics (MD) simulation results for low and moderate solvent densities ($\rho \leqslant 0.7$).[19] In addition, they also observed other interesting effects, such as an entropy-driven collapse transition for an athermal polymer/solvent system under certain conditions,[20] as well as collapse of a Lennard-Jones chain in a solvent near the critical point for sufficiently strong monomer-solvent attraction.[21] Mendez *et al.* also applied the hybrid MC/PRISM method to study the properties of polymer solutions for arbitrary polymer density using both simple[22] and atomistic[23] polymer/solvent models. More recently, Livadaru and Kovalenko introduced an alternative approach to study polymer solutions which combines the PRISM formalism with the polymer Green's function method.[24,25] In this approach, the intra- and intermolecular correlations are calculated in a self-consistent *analytical* manner, thereby bypassing the need to perform the computationally costly MC simulations and avoiding the associated statistical errors. They applied the method to study the behavior of alkanes in water and in the melt phase and found results that yielded overall good agreement with expected behavior and with other theoretical and experimental results.

The accuracy of the predictions from either the hybrid MC/PRISM method or the alternative approach of Refs. 24 and 25 is highly dependent on the validity of the various approximations implicit in the PRISM method (e.g., closure relations and equivalence of sites on the polymer), as well as that of the solvation potential. With respect to the latter, it should be noted that all the studies referred to the above utilize the pairwise additivity approximation in order to make the calculation tractable. While it is expected to become invalid in the limit of a dense, collapsed polymer under poor solvent conditions, this approximation could also be problematic even in good solvent conditions. The validity of this approximation was discussed over a decade ago by Grayce.[26] In that study, Grayce proposed as an alternative a simple many-body solvation potential (MBSP) for a polymer chain in a hard-sphere solvent. The potential is based on an extension of scaled particle theory (SPT) and is designed such that the effective potential energy depends on the surface area and volume of the cavity created by the polymer which is excluded to the centers of the solvent particles. The calculated monotonic decrease in the polymer size with increasing solvent density of a hard-sphere chain polymer was found to be quantitatively more precise than corresponding predictions using PRISM-HNC or PRISM-PY. In addition, many-body correlations were accurately predicted by the proposed potential. Despite the promising results of this study, there appears to have been no further investigation of this theoretical approach.

More recently, Taylor and co-workers investigated the validity of the pairwise-additive solvation potential approximation for short-chain polymer/solvent systems using an alternative form of the solvation potential.[7,8] While their proposed potential is pairwise additive, it differs from others of this type in that it consists of a *set* of pair potentials, where the form of each pair interaction is dependent on the number of monomers separating two sites along the chain. In addition, the pair potentials were generated using results from explicit-solvent simulations for 5-mers. Their potential was found to capture many of the solvent effects on the conformational behavior over a wider range of conditions than that considered in the study by Grayce. These studies suggest that the pairwise additivity approximation may not be the main source of the discrepancy between theory and simulation in earlier studies, as suggested in Ref. 26, but the forms of the particular potentials used, such as the HNC and PY potentials typically used in PRISM calculations.

The most effective means to test the accuracy of the theoretical predictions of polymer collapse is to compare them with results from MC and MD computer simulation studies that use the same polymer/solvent model. Early simulation studies of the coil-globule transition tended to employ isolated chain models in which the solvent effects were either ignored or implicitly incorporated into monomer-monomer (mm) interactions in an ill-defined manner. This approach had been followed because of the fact that explicit inclusion of solvent molecules in the simulations increases

considerably the computational cost of the calculations. With high solvent densities characteristic of real liquids, as well as the large simulation cell sizes required to minimize finite-size effects, large numbers of solvent particles are typically required. Consequently, most of the computational effort is then spent on the solvent itself. In recent years, however, explicit-solvent simulation studies have become more common.[27–40]

Early explicit-solvent simulation studies of collapse were helpful in elucidating the role of solvent entropy in the collapse transition. For example, an entropy-driven collapse transition was observed in studies using MC simulations with hard-particle polymer/solvent lattice models at sufficiently high solvent density.[27–29] For off-lattice explicit-solvent models of hard-sphere chains in a hard-sphere solvent, an entropy-driven collapse transition has also been observed but only for very large solvent/monomer size ratios[32] or nonadditive pair interactions.[33] For such models with monomer/solvent size ratios close to unity, the average chain size decreases monotonically with increasing solvent density,[41] but no collapse transition occurs perhaps due to the fact that it is pre-empted by the freezing transition of the solvent.

The phase behavior of polymer chains is more complicated for models employing attractive interactions in addition to hard-core or steeply repulsive short-range site-site interactions.[30,31,37–40] Luna-Bárcenas *et al.* investigated the behavior of Lennard-Jones chains in a supercritical monomeric solvent and observed collapse as the temperature was increased at constant pressure, with a transition temperature that was found to correlate well with the lower critical solution temperature of the corresponding polymer/solvent mixture at finite density. It was also noted that at sufficiently low temperatures, the polymer size *increases* with increasing solvent density, in contrast to the athermal (i.e., hard particle) limit. This effect arises from the screening of mm attractions by the solvent. Similar effects were also observed by Lísal and Nezbeda for hard-sphere/square-well polymer/solvent systems.[37,38]

More recently, our research group carried out simulation studies of the collapse transition for a polymer/solvent system employing Lennard-Jones-type interactions[39] and hard-sphere/square-well interactions.[40] While the models employed are very similar to those used in the studies of Refs. 30, 31, 37, and 38, a notable difference is that the collapse is driven by a variation in the energy mismatch in the attractions among monomers and solvent particles rather than by varying the temperature. In each study, the dependence of the coil-globule transition point on the solvent density was measured for two different model systems. In the first model, only mm interactions have an attractive component, and the variation in the strength of this attraction was used drive the collapse transition. It was observed that the magnitude of the attraction required to drive the collapse decreased monotonically with increasing solvent density. In the second model considered, mm, solvent-solvent (ss), and monomer-solvent (ms) interactions all have attractive components, though the ms attraction is variable and is used to control the effective solvent quality. Unlike the case for the first model, the transition point did not vary monotonically with changes in the solvent density. Screening of the mm attractions by the solvent tended to initially increase the stability of the coil state with solvent density, but this effect was reversed at high density where the entropic effects become more significant.[40]

The purpose of the present study is to investigate the accuracy of theoretical predictions of the polymer collapse transition. We report results for calculations that were carried out for two hard-sphere/square-well potential model systems and compare them to discontinuous MD (DMD) simulation results of Ref. 40. We have chosen to focus on two of several possible theoretical approaches: (1) the hybrid MC/PRISM method employing pairwise-additive HNC-type and PY-type solvation potentials and (2) the multibody potential proposed by Grayce.[26] In Sec. II we describe the two polymer/solvent model systems considered in this study. In Sec. III, we describe extensively the basic theoretical background and the technical details about implementing the methods to the model systems. Specifically, in Sec. III A we review the basic aspects of PRISM theory as well the form of the PRISM equation for the special case of a single chain considered here and the closure relations employed to solve the equation. Section III B presents a review of the derivation of the pairwise-additive solvation potentials employed in the PRISM calculations. Section III C discusses the technical details of implementing the MC/PRISM algorithm, and Sec. III D reviews the theoretical background of the multibody solvation potential of Ref. 26, as well as technical details concerning its use in MC simulations. The results of the calculations are presented and discussed in Sec. IV. Finally, in Sec. V we summarize the key results and conclusions.

II. MODEL

We consider two polymer/solvent models in this study. For each model, the polymer is composed of hard spherical monomers of diameter σ immersed in a solvent composed of hard spherical particles of the same size. The two models are distinguished by the nature of the ms, ss, and nonbonded mm interactions. In each model, some of the interactions have an attractive square well component in addition to the hard-core repulsive potential. The models are designed such that a tunable mismatch in the attractions controls the solvent quality and thus the preferred state of the polymer.

In model I, the three nonbonded interactions have the form,

$$\begin{aligned} u_{\mathrm{mm}}(r) &= \infty, && r < \sigma \\ &= -\lambda\epsilon, && \sigma < r < f\sigma \\ &= 0, && r > f\sigma, \end{aligned} \qquad (1)$$

$$\begin{aligned} u_{\mathrm{ms}}(r) = u_{\mathrm{ss}}(r) &= \infty, && r < \sigma \\ &= 0, && r > \sigma. \end{aligned}$$

Increasing the parameter λ increases the strength of the attraction between monomers and thus will drive the polymer to collapse. Note that f is the range of the mm attraction.

In model II, the interactions have the form,

$$u_{ms}(r) = \infty, \quad r < \sigma$$
$$= -(1-\lambda)\epsilon, \quad \sigma < r < f\sigma$$
$$= 0, \quad r > f\sigma \tag{2}$$
$$u_{mm}(r) = u_{ss}(r) = \infty, \quad r < \sigma$$
$$= -\epsilon, \quad \sigma < r < f\sigma$$
$$= 0, \quad r > f\sigma.$$

Note that f is the range of attraction for all three pair interactions. At $\lambda=0$, the attractions between the three pairs of particles are equal, corresponding to good solvent conditions. However, as λ increases, the mismatch in the energies of the different interactions also increases. It becomes more energetically favorable for the monomers and solvent particles to phase separate, i.e., for the polymer to collapse. Thus, in this model as well, increasing λ also tends to drive collapse. Consequently, we refer to λ as the hydrophobicity parameter for both models.

In addition to the nonbonded interactions, adjacent monomers on the polymer chain are bonded together with the following interaction:

$$u_{bond}(r) = 0, \quad |r-\sigma| < 0.1\sigma$$
$$= \infty, \quad |r-\sigma| > 0.1\sigma. \tag{3}$$

III. THEORY

A. PRISM theory

The general form of the PRISM equation is given by

$$\hat{\boldsymbol{H}}(k) = \hat{\boldsymbol{\Omega}}(k)\hat{\boldsymbol{C}}(k)[\hat{\boldsymbol{\Omega}}(k) + \hat{\boldsymbol{H}}(k)], \tag{4}$$

where $\hat{\boldsymbol{H}}$, $\hat{\boldsymbol{\Omega}}$, and $\hat{\boldsymbol{C}}$ are matrices whose elements are determined by the model system under consideration. In the present case, we consider a binary system composed of linear homopolymer chains, each of length N, in a solvent whose particles consist of a single interaction site. In this case, $\hat{\boldsymbol{H}}$, $\hat{\boldsymbol{\Omega}}$, and $\hat{\boldsymbol{C}}$ all reduce to 2×2 matrices. The elements of $\hat{\boldsymbol{H}}$ are given by

$$\hat{H}_{\alpha\beta}(k) = \rho_\alpha \rho_\beta \hat{h}_{\alpha\beta}(k), \tag{5}$$

where the subscripts α and β are labels for the monomer (m) or solvent (s) particles, ρ_α is the monomer or solvent site density, and where $\hat{h}_{\alpha\beta}(k)$ are the Fourier transforms of the total *intermolecular* pair correlation functions for mm, ms, and ss sites. Note that the correlation functions $h_{\alpha\beta}(r)$ are related to the corresponding pair distribution functions $g_{\alpha\beta}(r)$ according to

$$g_{\alpha\beta}(r) = h_{\alpha\beta}(r) + 1. \tag{6}$$

The elements of the matrix $\hat{\boldsymbol{C}}$, $\hat{c}_{\alpha\beta}(k)$, are the Fourier transforms of the intermolecular direct correlation functions between mm, ms, and ss site pairs. Finally, the elements of the matrix $\hat{\boldsymbol{\Omega}}(k)$ are Fourier transforms of the *intramolecular* distribution functions and are given by

$$\hat{\Omega}_{mm}(k) = \rho_m \hat{S}(k),$$
$$\hat{\Omega}_{ms}(k) = \hat{\Omega}_{sm}(k) = 0, \tag{7}$$
$$\hat{\Omega}_{ss}(k) = \rho_s \hat{S}_s(k),$$

where the intramolecular static structure factor of the polymer chain, $\hat{S}(k)$, is given by

$$\hat{S}(k) = 1 + \frac{1}{N}\sum_{i=1}^{N}\sum_{j=1\neq i}^{N}\left\langle \frac{\sin kr_{ij}}{kr_{ij}} \right\rangle, \tag{8}$$

where r_{ij} is the distance between sites i and j along the chain, and where the angular brackets denote an ensemble average over polymer conformations. In the special case considered in this study where the model solvent is composed of a single interaction site, the static structure factor for the solvent appearing in Eq. (7) is given by $\hat{S}_s(k)=1$.

In the present study, we are concerned with the conformational behavior of a single chain in a solvent. This corresponds to the limiting case where $\rho_m \to 0$. In this case, it is easy to show that two of the four equations implicit in the matrix equation (4) reduce to

$$\hat{h}_{ss}(k) = \hat{c}_{ss}(k) + \rho \hat{c}_{ss}(k)\hat{h}_{ss}(k), \tag{9}$$

$$\hat{h}_{ms}(k) = \hat{c}_{ms}(k)\hat{S}(k)[1 + \rho \hat{h}_{ss}(k)], \tag{10}$$

where we have dropped the subscript on the solvent density and now label it as ρ. Equation (9) is simple than the Ornstein–Zernicke equation for the single-site solvent whose solution yields the total and direct ss correlation functions. The solution of Eq. (10) yields the two ms correlation functions. This requires knowledge on $\hat{h}_{ss}$, which is obtained from the solution of Eq. (9), as well as the polymer chain structure factor $\hat{S}$. In addition, Eqs. (9) and (10) both require additional closure relations to relate the $\hat{h}_{\alpha\beta}$ and $\hat{c}_{\alpha\beta}$ correlation functions for ss and ms pairs. Noting that each of the pair potentials for the two models considered in this study have the general form of a hard-sphere component with or without an attractive square well, we choose to employ the the mean-spherical approximation (MSA) closure,

$$h_{\alpha\beta}(r) = -1, \quad r < \sigma,$$
$$c_{\alpha\beta}(r) = -\beta u_{\alpha\beta}(r), \quad r > \sigma. \tag{11}$$

The MSA closure is generally the most suitable simple atomic closure for potentials of this type where the the attractive component is short ranged.[42] In the case of model I, since $u_{ss}(r)$ and $u_{ms}(r)$ are both hard-sphere potentials [see Eq. (1)], this is identical to PY closure.

$$h_{ss}(r) = h_{ms}(r) = -1, \quad r < \sigma,$$
$$c_{ss}(r) = c_{ms}(r) = 0, \quad r > \sigma. \tag{12}$$

In the case of model II system, MSA closure, in combination with the pair potentials in Eq. (2), yields

$$h_{ss}(r) = -1, \quad r < \sigma,$$
$$c_{ss}(r) = \beta\epsilon, \quad \sigma < r < f\sigma$$
$$= 0, \quad r > f\sigma \tag{13}$$

and

$$h_{ms}(r) = -1, \quad r < \sigma,$$
$$c_{ms}(r) = \beta(1-\lambda)\epsilon, \quad \sigma < r < f\sigma$$
$$= 0, \quad r > f\sigma, \tag{14}$$

where $\beta = 1/k_B T$, k_B is the Boltzmann constant and T is temperature.

The choice of the PY closure relations of Eq. (12) is consistent with the approach taken in other PRISM studies of polymers in solution that have employed molecular models that only have short-range repulsive site-site interactions.[20–23] The authors of Refs. 24 and 25 studied a polymer-solvent system with attractive ms and ss interactions and employed a novel closure relation that was a combination of MSA and HNC closures. Such an approach could be used as an alternative to the purely MSA closure relations in Eqs. (13) and (14). A completely different approach to the atomiclike closures referred to here are the molecular closure relations introduced by Schweizer and Yethiraj,[43,44] which have been shown to be accurate for the thermodynamics of polymer blends and copolymers; however, it is unlikely that the advantages of this approach are relevant for the single-chain system studied here. Although the choice of closure relations is expected to have a quantitative influence on the results, we have chosen not to investigate the matter in this study.

The solution of $\hat{h}_{ms}(k)$ in Eq. (10) is complicated by the presence of the polymer chain structure factor. To address this problem, we use a standard procedure in which $\hat{h}_{ms}(k)$ and $\hat{S}(k)$ are determined self-consistently with the aid of a MC simulation for a single-polymer chain. The solvent is included implicitly through the introduction of a solvation potential. Below, we briefly review the theoretical basis of the solvation potentials employed in the present study.

B. PRISM solvation potentials

The configurational statistics of an N-monomer polymer immersed in a solvent composed of N_s single-site solvent particles is completely determined by the total configurational probability distribution,

$$\mathcal{P}_{N+N_s}(\mathbf{r}^N, \mathbf{r}'^{N_s}) = \frac{\exp[-\beta U_{N+N_s}(\mathbf{r}^N, \mathbf{r}'^{N_s})]}{Z_{N+N_s}}, \tag{15}$$

where Z_{N+N_s} is the normalization constant, $U_{N+N_s}(\mathbf{r}^N, \mathbf{r}'^{N_s})$ is the total potential energy of the polymer/solvent system, and where $\mathbf{r}^N \equiv \{\mathbf{r}_1, \mathbf{r}_2, \ldots, \mathbf{r}_N\}$ and $\mathbf{r}'^{N_s} \equiv \{\mathbf{r}'_1, \mathbf{r}'_2, \ldots, \mathbf{r}'_{N_s}\}$ are the sets of monomer and solvent coordinates, respectively. For the model systems considered in the present study, U_{N+N_s} can be written as

$$U_{N+N_s}(\mathbf{r}^N, \mathbf{r}'^{N_s}) = V_N(\mathbf{r}^N) + \sum_{i=1}^{N}\sum_{j=1}^{N_s} u_{ms}(|\mathbf{r}_i - \mathbf{r}'_j|) + \sum_{i<j}^{N_s} u_{ss}(|\mathbf{r}'_i - \mathbf{r}'_j|), \tag{16}$$

where $u_{ms}(r)$ and $u_{ss}(r)$ are the ms and ss pair potentials defined by Eq. (1) for model I and by Eq. (2) for model II. Further, the intramolecular potential energy of the polymer chain $V_N(\mathbf{r}^N)$ is given by

$$V_N(\mathbf{r}^N) = \sum_{i<j}^{N} u_{mm}(|\mathbf{r}_i - \mathbf{r}_j|) + \sum_{i=1}^{N-1} u_{bond}(|\mathbf{r}_{i+1} - \mathbf{r}_i|), \tag{17}$$

where $u_{mm}(r)$ is the mm pair potential in Eq. (1) or Eq. (2), and $u_{bond}(r)$ is the bonding potential in Eq. (3). The N-body conformational probability distribution for the polymer chain $\mathcal{P}_N(\{\mathbf{r}^N\})$ is obtained by integrating out the solvent coordinates,

$$\mathcal{P}_N(\mathbf{r}^N) = \int d\mathbf{r}'_1 \cdots d\mathbf{r}'_{N_s} \mathcal{P}_{N+N_s}(\mathbf{r}^N, \mathbf{r}'^{N_s}). \tag{18}$$

We can define the N-body solvation potential $W_N(\mathbf{r}^N)$ in terms of $V_N(\mathbf{r}^N)$ and $\mathcal{P}_N(\mathbf{r}^N)$ through the relation,

$$\mathcal{P}_N(\mathbf{r}^N) = \frac{\exp[-\beta(V_N(\mathbf{r}^N) + W_N(\mathbf{r}^N)\ ]}{Z_N}, \tag{19}$$

where Z_N is the corresponding normalization factor. The definition of W_N implies that the conformational behavior of a polymer chain in solution is exactly the same as that of an isolated chain subject to the intramolecular potential $V_N + W_N$.

The conformational behavior of the polymer chain is completely determined by $\mathcal{P}_N(\mathbf{r}^N)$ or, equivalently, by $W_N(\mathbf{r}^N)$. In principle, this distribution function can be calculated by solving Eqs. (15)–(19), but in practice this is an intractable problem, and approximations must be introduced. In the present study, we follow the approach taken in most other studies employing PRISM theory and consider a class of solvation potentials which are derived using the following approximations. First, The N-body solvation potential is taken to be pairwise additive,

$$W_N(\mathbf{r}^N) \approx \sum_{\alpha<\beta}^{N} W_2^{\alpha\beta}(r_{\alpha\beta}), \tag{20}$$

where $r_{\alpha\beta} \equiv |\mathbf{r}_\alpha - \mathbf{r}_\beta|$. The pair potentials in Eq. (20) are further assumed to be independent of the identities (i.e., location along the chain) of the monomer sites and dependent only on the distance between the sites, which we denote $W_2^{\alpha\beta}(r_{\alpha\beta}) \to w_{mm}(r_{\alpha\beta})$. Thus,

$$W_N(\mathbf{r}^N) \approx \sum_{\alpha<\beta}^{N} w_{mm}(r_{\alpha\beta}). \tag{21}$$

(In a more general version of this approximation, relevant for heteropolymers, there is a unique W_2 function for each monomer type pair.) An equivalent statement of this approximation is that the N-site indirect intramolecular correlation

function (or the "N-cavity distribution function"[45]), $y_N(\mathbf{r}^N) \equiv \exp[-\beta W_N(\mathbf{r}^N)]$, can be written as the product of indirect pair correlation functions,[45]

$$y_N(\mathbf{r}^N) \approx \prod_{\alpha<\beta}^{N} y_{\mathrm{mm}}(\mathbf{r}_{\alpha\beta}), \tag{22}$$

where $\ln y_{\mathrm{mm}}(r) = -\beta w_{\mathrm{mm}}(r)$. We interpret $y_{\mathrm{mm}}(r)$ as the indirect pair correlation function for two free (i.e., disconnected) monomers in the solvent, which is strictly correct only for the case of $N=2$ (i.e., a 2-site solute).[17] Noting that the pair distribution function of two such particles is given by

$$g_{\mathrm{mm}}(r) = e^{-\beta u_{\mathrm{mm}}(r)} y_{\mathrm{mm}}(r) = e^{-\beta(u_{\mathrm{mm}}(r)+w_{\mathrm{mm}}(r))}, \tag{23}$$

it therefore follows that

$$-\beta w_{\mathrm{mm}}(r) = \ln g_{\mathrm{mm}}(r) + \beta u_{\mathrm{mm}}(r). \tag{24}$$

The derivation of an expression for $w_{\mathrm{mm}}(r)$ now hinges on the approach taken to determine the pair distribution function $g_{\mathrm{mm}}(r)$ for two free monomer sites in a solvent. The potentials considered in this study are derived employing the Ornstein–Zernicke equation for binary mixtures of free monomers and solvent sites in the limit of zero monomer density, together with suitable closure relations. Note that for multisite solvent molecules, the RISM equation should be used.[17]

Using the HNC approximation,

$$\ln g_{\mathrm{mm}}(r) = -\beta u_{\mathrm{mm}}(r) + h_{\mathrm{mm}}(r) - c_{\mathrm{mm}}(r), \tag{25}$$

the solvation pair potential in Eq. (24) becomes

$$-\beta w_{\mathrm{mm}}(r) = h_{\mathrm{mm}}(r) - c_{\mathrm{mm}}(r). \tag{26}$$

In the limit of zero monomer density, it is easy to show that the Ornstein–Zernicke equation for binary mixtures yields

$$h_{\mathrm{mm}}(r) = c_{\mathrm{mm}}(r) + c_{\mathrm{ms}}(r) * \chi_{\mathrm{ss}}(r) * c_{\mathrm{sm}}(r), \tag{27}$$

where $\chi_{\mathrm{ss}}(r) = \rho[\delta(r) + \rho h_{\mathrm{ss}}(r)]$, and where "$f * g$" represents a convolution between functions $f(r)$ and $g(r)$. Consequently,

$$\beta w_{\mathrm{mm}}(r) = -c_{\mathrm{ms}}(r) * \chi_{\mathrm{ss}}(r) * c_{\mathrm{sm}}(r). \tag{28}$$

[Note that the two ms direct correlation functions are symmetric upon subscript exchange: $c_{\mathrm{ms}}(r) = c_{\mathrm{sm}}(r)$.] We refer to the solvation potential in Eq. (28) as the HNC-type potential because its derivation employs that closure relation. This potential was first derived by Chandler and co-workers in their study of the "conformational" changes in a zero-thickness polymer isomorphic to a quantum solvated electron.[16,46]

As an alternative, the PY closure relation

$$g_{\mathrm{mm}}(r) = e^{-\beta u_{\mathrm{mm}}(r)}[1 + h_{\mathrm{mm}}(r) - c_{\mathrm{mm}}(r)] \tag{29}$$

can be used instead with Eqs. (24) and (27) to yield the PY-type potential,

$$\beta w_{\mathrm{mm}}(r) = -\ln[1 + c_{\mathrm{ms}}(r) \times \chi_{\mathrm{ss}}(r) \times c_{\mathrm{sm}}(r)]. \tag{30}$$

This PY-type potential was first derived by Grayce and Schweizer.[17]

C. Implementation of the PRISM-MC method

The quantities of interest in this study are those relating to conformational properties of the polymer chain, such as the radius of gyration R_g and the scaling exponent ν. These conformational properties are completely determined by the N-site monomer probability distribution $\mathcal{P}_N(\mathbf{r}^N)$, defined with respect to the total $(N+N_s)$-site probability distribution in Eq. (18). The distribution $\mathcal{P}_N(\mathbf{r}^N)$, in turn, is determined by the solvation potential, $W_N(\mathbf{r}^N)$, from Eq. (19). Using the approximation for $W_N(\mathbf{r}^N)$ in Eq. (21), it is clear that the conformational behavior of the chain in solution is identical to that of an isolated chain in vacuum subject to the bonding potential of Eq. (3) and an effective pair potential for nonbonded monomers given by

$$u_{\mathrm{tot}}(r) = u_{\mathrm{mm}}(r) + w_{\mathrm{mm}}(r), \tag{31}$$

where $u_{\mathrm{mm}}(r)$ is the true nonbonded mm pair potential given by Eq. (1) for model I and by Eq. (2) for model II, and where $w_{\mathrm{mm}}(r)$ is either of the two potentials of Eqs. (28) and (30). The conformational properties of the chain are measured by carrying out a single-chain MC simulation using the effective potential for nonbonded monomers in Eq. (31), in addition to the bonding potential of Eq. (3). Calculation of the potentials using Eqs. (28) and (30) requires $c_{\mathrm{ms}}(r)$. This is obtained by solving Eq. (10) together with the closure relation [Eq. (11)]. Note that the function $h_{\mathrm{ss}}(r)$ appearing in Eq. (10) is obtained from solving Eq. (9). However, as previously noted, the solution to Eq. (10) is complicated by the fact that this equation depends on the static structure factor of the polymer chain, $\hat{S}(k)$. The structure factor is obtained from the single-chain MC simulation. Since the simulation uses the solvation potential, which depends on the structure factor, a self-consistent calculation must be carried out over a sufficient number of iterations, each involving a MC simulation to calculate $\hat{S}(k)$ and the solution of Eq. (10) with the suitable closure relation until satisfactory convergence in the correlation functions is achieved. In addition to providing the conformational properties of the chain, this method also yields predictions for the ms distribution function, $g_{\mathrm{ms}}(r) \equiv h_{\mathrm{ms}}(r) + 1$, through the solution of Eq. (10).

We employ the pivot algorithm in the MC simulation to generate the trial chain configurations. In our implementation of this algorithm, we choose a random monomer that divides the chain into two parts. One part of the chain is rotated in either one of the two ways. First, the bond angle θ defined at the site of the randomly chosen monomer is varied by a random increment in $\delta(\cos\theta)$, chosen from a uniform distribution in the full range $\delta(\cos\theta) \in (-1, 1)$. Second, the azimuthal angle ϕ about a bond containing the randomly chosen monomer was randomly incremented by an amount $\delta\phi$, chosen from a uniform distribution in the range $\delta\phi \in (-\pi, \pi)$. Since bond lengths of the model polymer are of variable length and each of the rotations leaves the bond lengths unchanged, additional moves must be carried out. We chose to use a simple random displacement move, in which each of the Cartesian coordinates of a randomly chosen monomer are incremented by an amount Δ that is drawn from a uniform distribution in the range $\Delta \in (-\Delta_{\max}, \Delta_{\max})$, where

$\Delta_{max}=0.15\sigma$. The two chain-segment rotations and the monomer displacements were generated with equal probability and accepted according to the Metropolis algorithm. The veracity of implementation of the MC simulation procedure was checked in several ways. For short chains (i.e., $N=3,4,5$), various quantities such as the mean-square radius of gyration and the end-to-end distance were measured using the procedure outlined above and a variant of the procedure with only the random particle displacements and no pivot algorithm moves. The results were found to be identical, which provides strong evidence that the pivot algorithm moves were properly implemented. In addition, results from simulations of $N=3$ and $N=4$ hard-sphere chains with fixed-bond length, using only the two bond rotation moves, were compared to those from MC simulations by Taylor[6] and were found to be in agreement. Finally, simulation results for fixed-bond trimers with various solvation potentials were consistent with "exact" results calculated by numerical integration. With these and various other checks, we are confident that the single-chain MC simulations were properly carried out.

The initial chain configuration in each MC simulation was chosen from a previous calculation at the same hydrophobicity parameter value λ and solvent density ρ. If this was not available, then it was generated from a self-avoiding random walk. Each simulation consisted of an equilibration run of approximately 10^5 MC cycles, followed by a production run of 2×10^6 MC cycles. In the final iteration of the self-consistent method, a longer production run of 10^7 MC cycles was used. A single MC cycle, on average, consisted of an attempted change in the bond angle, azimuthal angle, or Cartesian coordinates of a randomly chosen monomer, each with equal probability. Sampling of $\hat{S}(k)$ occurred typically every 1000 MC cycles and was discretized in k-space over 4096 points in increments of $\Delta k=2\pi/\Delta r$, where the real-space increment was chosen to be $\Delta r=0.01\sigma$.

The two PRISM equations (9) and (10) were solved using the simple Picard integration scheme with fast Fourier transforms. Defining $\gamma_{\alpha\beta}(r)\equiv h_{\alpha\beta}(r)-c_{\alpha\beta}(r)$ the Fourier transforms of PRISM equations can be written as

$$\hat{\gamma}_{ss}(k)=\rho(\hat{c}_{ss}(k))^2/(1-\rho\hat{c}_{ss}(k)), \tag{32}$$

$$\hat{\gamma}_{ms}(k)=\hat{c}_{ms}(\hat{S}(k)-1+\rho\hat{h}_{ss}(k)), \tag{33}$$

and the closure relations of Eq. (11) can be written as

$$\begin{aligned} c_{\alpha\beta}(r) &= -\gamma_{\alpha\beta}(r)-1, \quad r<\sigma \\ &= -\beta u_{\alpha\beta}(r), \quad r>\sigma, \end{aligned} \tag{34}$$

where, in the latter range of r, $u_{\alpha\beta}(r)=0$ except for the ms potential of model II. An initial guess for $h_{\alpha\beta}(r)$ was used to generate a corresponding initial estimate for $c_{\alpha\beta}(r)$ using Eq. (10). These two functions together provide an initial estimate of $\gamma_{\alpha\beta}(r)$, which we call $\gamma^{in}_{\alpha\beta}(r)$. The equations were then solved self-consistently in the following manner: (i) applying the closure relation of Eq. (34) to find $c_{\alpha\beta}(r)$; (ii) calculating the Fourier transform, $\hat{c}_{\alpha\beta}(k)$; (iii) solving Eq. (32) or Eq. (33) to find $\hat{\gamma}_{\alpha\beta}(k)$; (iv) calculating the inverse Fourier transform to find a revised estimate of $\gamma_{\alpha\beta}(r)$, which we call $\gamma^{out}_{\alpha\beta}(r)$; and (v) employing the Broyles mixing scheme[47] by weighing original estimate, $\gamma^{in}_{\alpha\beta}(r)$, and the new estimate, $\gamma^{out}_{\alpha\beta}(r)$, to generate a new estimate for $\gamma^{in}_{\alpha\beta}(r)$,

$$\zeta\gamma^{in}_{\alpha\beta}(r)+(1-\zeta)\gamma^{out}_{\alpha\beta}(r)\rightarrow\gamma^{in}_{\alpha\beta}(r), \tag{35}$$

and using this as trial input by cycling back to step (i). Typically, a mixing parameter value of $\zeta=0.95$ was used. The self-consistent calculations continued until the condition $|1-\gamma^{out}_{\alpha\beta}(r)/\gamma^{in}_{\alpha\beta}(r)|<10^{-14}$ was reached. This set of calculations was carried out for each step in the full MC/PRISM self-consistent calculation for the solution of Eq. (33) since Eq. (33) requires an updated estimate of $\hat{S}(k)$ from the simulation. However, since Eq. (32) is independent of $\hat{S}(k)$, it was necessary to carry out the calculations only once to find $h_{ss}(r)$. For any given λ and ρ, $\hat{h}_{ss}(k)$ was used as the initial trial input for $\hat{h}_{ms}(k)$ in Eq. (10).

D. SPT solvation potential: Theory and implementation

Consider a hard-sphere polymer chain in a specific conformation with the corresponding monomer coordinates $\{\mathbf{r}^N\}$. In the presence of a hard-sphere solvent, the polymer creates a cavity whose volume is excluded to the centers of the solvent particles. The cavity is composed of a collection of overlapping spheres, one for each monomer. The MBSP introduced by Grayce in Ref. 26 has the general form,

$$W_N(\mathbf{r}^N)=pV_c+\gamma S_c, \tag{36}$$

where V_c and S_c are the volume and surface area, respectively, of the cavity from which the solvent particle centers are excluded, p is the solvent pressure, and γ is the surface tension of the solvent-cavity interface. Note that the solvation potential is inherently a many-body potential, in contrast to the pairwise-additive potentials considered earlier in the context of PRISM theory. The solvation potential is also equivalent to the reversible work required to create a cavity of a specified size and shape in the solvent. The solvent pressure p is calculated using the Carnahan–Starling equation of state for hard spheres,

$$\frac{p}{\rho k_BT}=\frac{1+\phi+\phi^2+\phi^3}{(1-\phi)^3}, \tag{37}$$

where $\phi\equiv(\pi/6)\rho\sigma^3$ is the volume fraction of the solvent. The surface tension γ is calculated using SPT and is assumed to be equal to that calculated for a spherical cavity in a hard-sphere fluid. Because the overlapping excluded-volume spheres making up the full cavity have a high degree of curvature, the surface tension is assumed to have the form,

$$\gamma=\gamma_0(1-\xi\sigma/r). \tag{38}$$

The quantity r is the radius of a spherical cavity excluded to the solvent by each monomer. Since the monomer and solvent particles in the models considered in the present study are equal in size, the cavity radius is equal to σ, the monomer and solvent particle diameter. The basic methods of SPT can be applied to calculate the parameters γ_0 and ξ (see, for

example, pp. 51–55 of Ref. 48). Using this approach, it can be shown that

$$\beta\gamma_0\sigma^2 = -\frac{9\phi^2(1+\phi)}{2\pi(1-\phi)^3} \tag{39}$$

and

$$\xi = \frac{\phi}{1+\phi}. \tag{40}$$

Equations (36)–(40) constitute the MBSP solvation potential of Grayce.

In order to utilize the MBSP potential, we require a procedure for the rapid calculation of the volume of the excluded-volume cavity V_c and surface area S_c. Rather than following the procedure outlined by Grayce in the appendix of Ref. 26, we used the algorithm developed by Busa *et al.*[49] The ARVO FORTRAN package developed by Busa *et al.* was slightly modified so that it could be incorporated into a MC simulation program for a polymer chain.

Single-chain MC simulations were performed using an effective potential given by the sum,

$$U_N^{\text{eff}}(\mathbf{r}^N) = V_N(\mathbf{r}^N) + W_N(\mathbf{r}^N), \tag{41}$$

where the pairwise-additive intramolecular potential energy $V_N(\mathbf{r}^N)$ is given by Eq. (17) and where the MBSP potential $W_N(\mathbf{r}^N)$ is given by Eqs. (36)–(40). As was the case for the PRISM calculations, the MC simulations using the MBSP potential were carried out using the pivot algorithm, with the same angle-bending rotations, torsional rotations, and random-monomer displacements described in Sec. III C. Acceptance of the moves was determined using the Metropolis criterion. Unlike the procedure followed for the PRISM simulations, no self-consistent calculations were required for the MBSP simulations; rather, only a single MC simulation was required for each state point. Consequently, the simulations tended to proceed more quickly than was the case for PRISM. Prior to carrying out the calculations used to generate the results given in Sec. IV, we first tested our MC program by performing calculations identical to those conducted in Ref. 26 for hard-sphere 3-mers and 10-mers with fixed-bond lengths in a hard-sphere solvent for various densities. Our calculated mean-square end-to-end distance R_e^2 was exactly the same as those reported by Grayce. Subsequently, MBSP calculations were carried out using model I polymer/solvent model system for solvent densities ranging from $\rho=0$ to $\rho=0.9$ and hydrophobicity parameter values ranging from $\lambda=0$ to $\lambda=1$. Each simulation consisted of an equilibration run of approximately 10^4 MC cycles, followed by a production run of 2×10^6 MC cycles, where a single MC cycle consisted of an attempted change in the bond angle, azimuthal angle, or Cartesian coordinates of a randomly chosen monomer.

E. Locating the transition

In the limit of sufficiently long chain length, the physical size of a polymer obeys the well-known scaling relation,

$$R \sim N^{\nu}, \tag{42}$$

where N is the number of statistical segments of the polymer. An important example of polymer size is the average radius of gyration of the polymer $\bar{R}_g$ defined as

$$\bar{R}_g \equiv \sqrt{\langle R_g^2\rangle} \equiv \sqrt{\frac{1}{N}\sum_{n=1}^{N}\langle|\vec{R}_n - \langle\vec{R}\rangle|^2\rangle}, \tag{43}$$

where $\vec{R}_n$ is the position of monomer n, $\langle\vec{R}\rangle$ is the average monomer position, and where the angular brackets denote a statistical averaging over polymer conformations. In the limit of large N, the scaling exponent assumes specific values, which characterize the state of the polymer chain, and which are independent of the details of the interactions in the system. When the polymer is in the swollen coil state under good solvent conditions, $\nu\approx0.5876$.[50–52] Conversely, in poor solvent conditions, the polymer will be in the compact liquidlike globule state with $\nu=\frac{1}{3}$. Near the polymer collapse transition, the conformational statistics of the polymer are close to those of an ideal chain, where the scaling exponent is given by $\nu=\frac{1}{2}$. Note that the collapse transition for a polymer chain with pairwise-additive potential energy is typically defined to occur at the point where the second virial coefficient vanishes, i.e.,

$$B_2 = 2\pi\int_0^{\infty} drr^2(1-\exp[-\beta u(r)]) = 0, \tag{44}$$

where $u(r)$ is the mm pair potential. For the PRISM calculations in the present study, the condition in Eq. (44) with the total effective potential given in Eq. (31) can be used in place of $u(r)$ in the equation above. Note, however, that this is not possible for the MBSP calculations since the corresponding solvation potential is not pairwise additive; consequently, there is no effective *pair* potential that can be used to calculate B_2 in Eq. (44). However, an important goal of this study is a comparison of the theoretical predictions with the explicit-solvent DMD simulation results in Ref. 40. Since the collapse transition in that study was chosen to be defined by the ideal-chain condition (since the $\nu=\frac{1}{2}$ criterion is obtained directly from the simulation results, unlike the condition $B_2=0$), we adopt that convention here as well. While the difference between the transition points calculated in these different ways scales with the chain length as $N^{-1/2}$ and thus vanishes in the thermodynamic limit, the difference is nonnegligible for the $N=30$ chains considered here. We return to this matter in Sec. IV, where we compare coil-globule phase boundaries for model I system calculated using both conventions.

In order to locate the transition point, we determine where the ideal-chain condition $\left(\nu=\frac{1}{2}\right)$ holds using the same procedure employed in the DMD simulation study of Ref. 40, as well as the related MD study in Ref. 39. This approach uses the fact that the static structure factor $S(\vec{k})$ of a polymer chain, defined in Eq. (8), satisfies the relation

$$S(k) \propto k^{-1/\nu} \tag{45}$$

in the limit where $R_g^{-1} \ll k \ll \sigma^{-1}$, where σ is simultaneously (for the model employed here) the monomer size and the

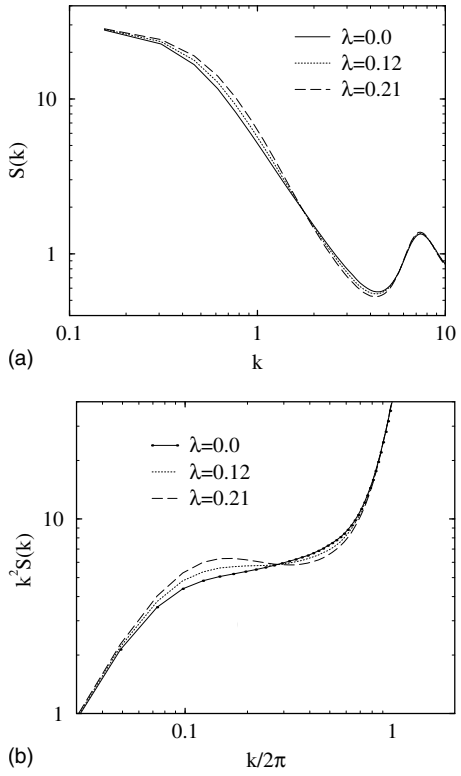

FIG. 1. (a) Structure factor functions $S(k)$ for a polymer of length $N=30$. These data were calculated for model I at a density of $\rho=0.8$, a temperature of $T=1.0$ at the three values of the hydrophobicity parameter, λ, indicated in the figure. The calculations were performed using the HNC-type solvation potential. (b) The same three structure factors shown in graph (a) plotted in the standard Kratky form.

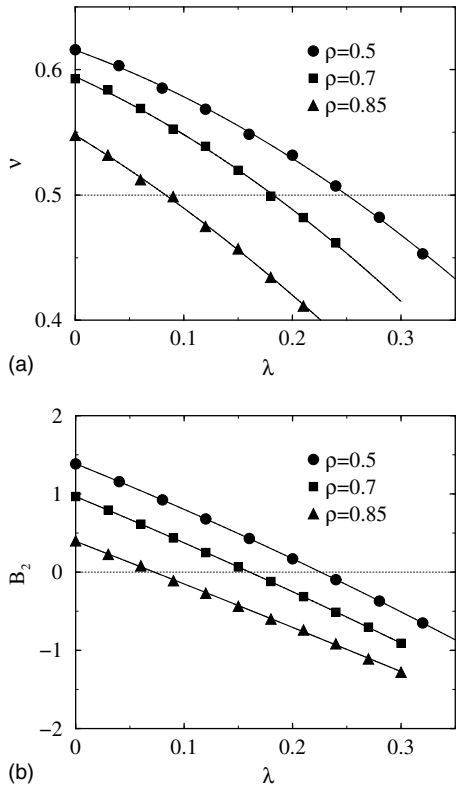

FIG. 2. (a) Calculated scaling exponent ν vs hydrophobicity parameter λ. The scaling exponents were calculated by fitting the static structure factor to Eq. (45) in the range $k\in[1.0,1.8]$. These data were obtained for model I for a polymer of length $N=30$, a temperature of $T=1.0$ at the three solvent densities indicated in the figure. The HNC-type solvation potential was employed. The solid lines are fits of the data to a quadratic polynomial. The intersection of the curves with the $\nu=\frac{1}{2}$ dotted line yield the λ_{id} values corresponding to the collapse transition point. (b) Corresponding plots of the second monomeric virial coefficient B_2 vs λ. The intersection of the curves with the $B_2=0$ dotted line yield the λ values corresponding to the collapse transition point.

bond length. Note that this condition is only satisfied for sufficiently long chains, for which $R_g \gg \sigma$. In the present case, where $N=30$, the chains are clearly too short to rigorously satisfy the condition. On the other hand, as is evident in the sample calculated structure factor plotted on the log-log graph in Fig. 1(a), there is a linear regime apparent in the range $R_g^{-1} \lesssim k \lesssim \sigma^{-1}$. Note that the scaling exponent satisfies the relation $\nu=-1/m$, where m is the slope of this linear regime. Figure 1(b) shows the same three structure factors plotted in standard Kratky form and illustrates the collapse of the chain with increasing λ more clearly than is evident in Fig. 1(a) by the growth in a peak near $k/(2\pi)=0.15$. For the calculations performed in this study, we determined ν by fitting $S(k)$ using Eq. (45) in the range $\ln k\in[1.0,1.8]$, where the predicted scaling of $S(k)$ was found to be accurate from $\lambda=0$ ("maximally good" solvent conditions) to just below λ_{id}, the value of λ for which $\nu=\frac{1}{2}$. (Note that in poor solvent conditions, where R_g is small, the chain length $N=30$ precludes the existence of a range of k where the scaling relation holds.) In this manner, we measured ν as a function of the hydrophobicity parameter λ. To determine each λ_{id} value, the data were first fitted to a quadratic polynomial; typical fits are shown in Fig. 2(a). While we expect there to be non-negligible finite-size effects, the calculated coil-globule phase boundaries should display the general qualitative features present for longer-chain systems. For comparison, we also show corresponding plots of B_2 versus λ in Fig. 2(b). Note that the λ values for which $\nu=\frac{1}{2}$ differ slightly from those predicted from the $B_2=0$ condition. This discrepancy is expected to vanish in the limit of $N\to\infty$.

In addition to the calculations of the coil-globule phase boundaries using the MC/PRISM self-consistent method with the condition $\nu=\frac{1}{2}$ as determined by an analysis of the static structure factor, we also show predicted phase boundaries calculated using a simple Flory-type theory that were previously shown in Ref. 40, to which the reader may refer for further details.

IV. RESULTS AND DISCUSSION

A. Model I

Figure 3 shows plots of the mean-square radius of gyration R_g^2 versus degree of hydrophobicity λ for model I polymer/solvent system for a chain of length $N=30$. Results for four different densities obtained using PRISM calculations with a HNC-type solvation potential (PRISM-HNC), PRISM calculations with a PY-type solvation potential (PRISM-PY), and MC simulations with the MBSP potential, are shown in Figs. 3(a)–3(c), respectively. In each graph, the theoretical data are overlaid on results obtained from explicit-solvent DMD simulation data collected in our previous study.[40] The general qualitative trends for the three the-

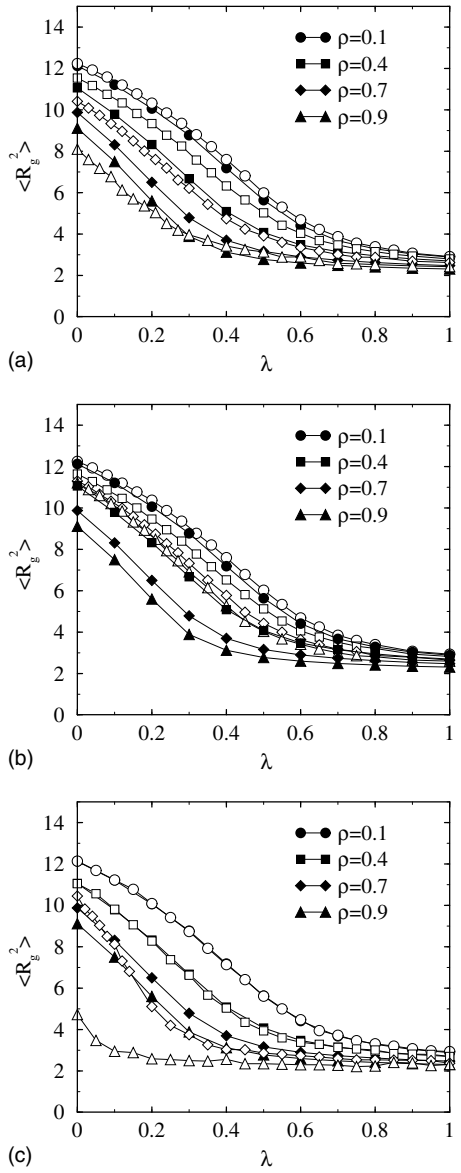

FIG. 3. (a) Mean-square radius of gyration $\langle R_g^2 \rangle$ vs hydrophobicity parameter λ for model I with a polymer of length $N=30$, a range of attraction of $f=1.5$, and at a temperature of $T=1.0$. The open symbols correspond to calculations using the PRISM theory with the HNC-type potential of Eq. (28). The closed symbols correspond to data from explicit-solvent DMD simulations from Ref. 40 for the same polymer-solvent system. (b) Same as in (a) except that the data for the open symbols correspond to calculations using the PY-type potential of Eq. (30). (c) Same as in (a) except that the data for the open symbols correspond to calculations using the MBSP potential of Eq. (36).

oretical calculations are consistent with those observed for the explicit-solvent simulations: (1) the average size of the polymer chain decreases with increasing hydrophobicity λ (which for model I is simply the strength of attraction between pairs of monomers) and (2) the average size decreases monotonically with increasing density of the hard-sphere solvent. However, there are notable quantitative differences among the three sets of theoretical results. The PRISM-HNC calculations yield R_g^2 values that tend to overestimate the DMD values except for the case of very high solvent density and relatively low values of λ, where it underpredicts R_g^2. The PRISM-PY calculations yield results that consistently

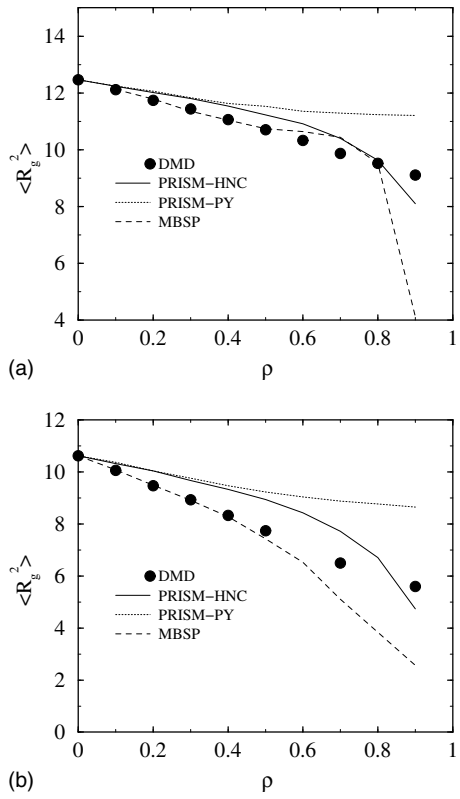

FIG. 4. (a) Mean-square radius of gyration $\langle R_g^2 \rangle$ vs solvent density ρ for model I with chain length $N=30$, hydrophobicity $\lambda=0$, range of attraction $f=1.5$, and a temperature of $T=1.0$. Theoretical calculations using HNC, PY, and MSBP potentials of Eqs. (28), (30), and (36), respectively, are overlaid on explicit-solvent DMD simulation data from Ref. 40. (b) As in (a) except $\lambda=0.2$.

overestimate the DMD values. The magnitude of the discrepancy is comparable to that of PRISM-HNC at low densities ($\rho \leqslant 0.4$) but becomes considerably greater at medium to high solvent density ($\rho > 0.4$). Thus, the HNC-type potential is always at least as good as the PY-type potential for PRISM calculations and is significantly better at high density, which is the physically relevant regime for a true liquid solvent. (Note, however, that the medium- to low-density regimes in these calculations are still physically relevant for polymer/colloid mixtures since the "solvent" particle of the present calculations can also be interpreted as a colloidal particle.) The MBSP calculations yield results that are near perfect for lower densities ($\rho \leqslant 0.5$) but which increasingly overestimate the compressive effects of the solvent on the polymer at higher densities. This discrepancy appears to increase with increasing chain length, as the $N=30$ MBSP results in Fig. 3(c) show a polymer which is fully collapsed for all λ, including $\lambda=0$, the limiting case where mm, ms, and ss interactions are all of hard-sphere type. Thus, the MBSP potential predicts an entropy-driven phase transition at high solvent density, a phenomenon which is clearly not observed in the explicit-solvent DMD calculations.

Figure 4 shows a comparison between the theoretical predictions and the corresponding explicit-solvent results of the mean-square radius of gyration $\langle R_g^2 \rangle$ versus solvent density for a $N=30$ chain. Figure 4(a) shows the case of $\lambda=0$, which corresponds to the athermal limiting case for model I

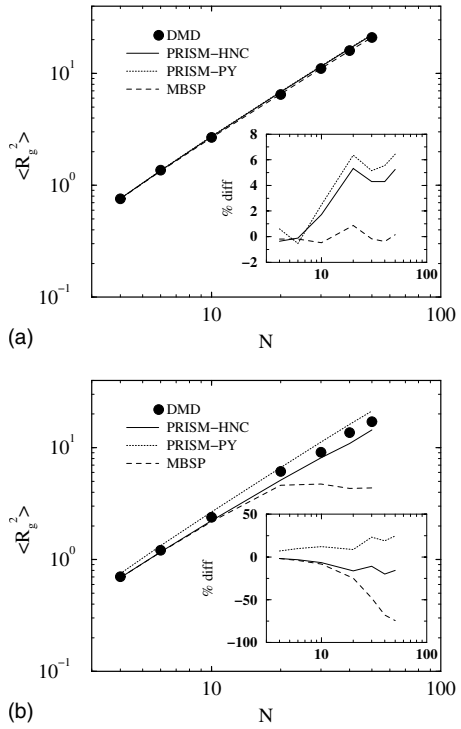

FIG. 5. (a) Mean-square radius of gyration $\langle R_g^2 \rangle$ vs chain length N for model I at a solvent density of $\rho=0.4$. The hydrophobicity value is $\lambda=0$, which corresponds to the athermal limit for model I, i.e., a hard-sphere chain in a hard-sphere solvent. The inset shows the % difference between each of the three theoretical predictions and the values from explicit-sovlent DMD simulations, i.e., % difference $\equiv \langle R_g^2(\text{theory}) - R_g^2(\text{DMD}) \rangle / \langle R_g^2(\text{DMD}) \rangle \times 100$. (b) As in (a) except $\rho=0.9$.

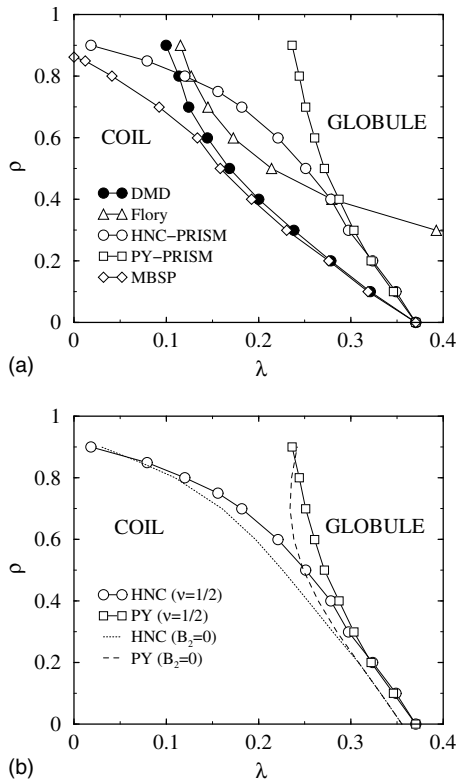

FIG. 6. (a) Coil-globule phase boundaries for model I with a polymer of length $N=30$, a range of attraction of $f=1.5$, and at a temperature of $T=1.0$. The explicit-solvent DMD simulation data of Ref. 40 are shown as filled circles. Theoretical predictions from a Flory-type theory (open triangles), PRISM theory with the HNC-type potential of Eq. (28) (open circles) and with the PY-type potential of Eq. (30) (open squares), as well as the MBSP potential of Eq. (36), are also shown. All theoretical curves were calculated using the criterion that $\nu=\frac{1}{2}$, where ν is the scaling exponent calculated from an analysis of the static structure factor. (b) Phase boundaries calculated using PRISM-HNC and PRISM-PY potentials using the criterion that $\nu=\frac{1}{2}$ [same data as in (a) above] and using the criterion that $B_2=0$, where B_2 is the effective second virial coefficient calculated using Eq. (44) with the total effective potential $u_{\text{tot}}(r)$ of Eq. (31).

of a hard-sphere chain in a hard-sphere solvent. At this value of λ, the average chain size is at its maximum for each density. As in Fig. 3, we note that the MBSP prediction is nearly exact for low to moderate densities ($\rho \leqslant 0.5$). At higher densities, it overestimates $\langle R_g^2 \rangle$ up to $\rho=0.8$, beyond which it dramatically *underestimates* $\langle R_g^2 \rangle$. This is consistent with the results shown in Fig. 3(c). Thus, the MBSP potential overestimates the compressive effects of the solvent on the chain at high ρ and falsely predicts an entropy-driven collapse transition upon an increase in the solvent density. By contrast, the PRISM-HNC and PRISM-PY theories provide poorer predictions at lower to moderate densities but are not quite as poor as MBSP at very high density. Figure 4(b) shows similar theoretical results for the same system except with a hydrophobicity of $\lambda=0.2$, a value that is close to the transition point for all solvent densities. The trends are similar to those for $\lambda=0$.

It is instructive to investigate the scaling behavior of the polymer size predicted by each of the three different theoretical approaches. Figure 5 shows the theoretical predictions for the variation in $\langle R_g^2 \rangle$ with chain length N for PRISM-HNC, PRISM-PY, and MBSP, as well as the explicit-solvent simulation data obtained from DMD simulations. Results are shown for solvent densities of (a) $\rho=0.4$ and (b) $\rho=0.9$. The inset shows the % difference between each theory and the exact results, which more clearly distinguishes the relative quantitative accuracy of each theory. At $\rho=0.4$, the generally good agreement between the predictions of each theory and the exact results is apparent. All three theories yield quantitatively precise predictions for very short chain lengths. However, for longer chain lengths, the accuracy of the PRISM calculations worsens somewhat, while the MBSP calculation is consistently accurate. For $\rho=0.9$, the trends are noticeably different. For short chain lengths the PRISM-HNC and MBSP calculations are both fairly accurate, while the PRISM-PY calculations are considerably poorer. Upon an increase in the polymer chain length, the accuracy of all theoretical predictions worsen, with PRISM-PY overestimating, and PRISM-HNC and MBSP predictions underestimating the polymer size. At the longest chain lengths considered ($N=50$), the MBSP estimates of $\langle R_g^2 \rangle$ are the least accurate of the three predictions.

Figure 6(a) shows the coil-globule phase boundary calculated for a polymer of length $N=30$ using the procedure outlined in Sec. III E, in which the $\nu=\frac{1}{2}$ criterion was applied to the static structure factor data. Again, the theoretical predictions obtained from PRISM-HNC, PRISM-PY, and MBSP calculations are shown along with the phase boundary predicted using the same criterion for the DMD data. In addition, we have included a theoretical prediction obtained us-

ing a simple Flory-type mean-field theory. Both the DMD results and the Flory-type theoretical predictions were presented in our earlier study,[40] to which the reader should refer for greater detail. Once again, the theoretical predictions are all qualitatively consistent with the exact DMD result that the λ values at the transition point decrease monotonically with increasing density. (Note that for model I, varying λ at fixed temperature is equivalent to varying the reciprocal of the temperature for fixed λ. Consequently, an alternative description of the phase diagram is that the transition temperature increases monotonically with increasing solvent density.) Thus, increasing the density of the hard-sphere solvent tends to stabilize the globule state with respect to the coil state of the polymer, a fact which is also clearly visible from the plots of R_g^2 versus λ in Fig. 3. As discussed at length in Ref. 40, this effect can be easily understood as an increase in the free volume (and thus translational entropy) of the hard-sphere solvent that apparently correlates with a decrease in the average polymer size. The difference between the solvent entropy associated with the coil and globule states increases with increasing solvent density and favors the globule over the coil state with increasing density, a fact first noted by Dijkstra and co-workers.[27,28]

Like the Flory theory predictions for the coil-globule phase boundary that were first presented in Ref. 40, the PRISM and MBSP predictions in the present study are mostly qualitatively consistent with the explicit-solvent DMD simulation results. However, it must be noted that the latter theoretical approaches are fundamentally different in character from the Flory approach. This difference is reflected in certain trends in the data, for example, the fact that the PRISM-HNC, PRISM-PY, MBSP, and DMD data all converge at $\rho=0$, while the Flory-theory curve does not. This trend is relatively easy to understand and arises from the fact that the results of the former group all involve simulations of a single-polymer chain with identical intramolecular interactions, plus additional interactions arising from the solvent that are either exact (DMD) or approximate (PRISM-HNC, PRISM-PY, and MBSP). In the limit where $\rho\to 0$, the effective interactions due to the solvent particles vanish for all four cases, and the simulation models are exactly the same. By contrast, the Flory-type theory takes an entirely different approach which does not involve a single-chain simulation from which the scaling exponent ν is extracted from an analysis of the structure factor. Rather, it employs an approximate free energy function $F(\alpha)$, which is minimized with respect to $\alpha \equiv R_g/R_{g,\theta}$, where $R_{g,\theta}$ is the value of R_g at the theta point and is subjected to the condition that $\sqrt{\langle \alpha^2 \rangle}=1$ at the transition (see Ref. 40 for further details). Given the approximate form of $F(\alpha)$ and the different criteria employed to calculate the transition point (which will be equivalent to the $\nu=\frac{1}{2}$ criterion in the thermodynamic limit, but not for the case of finite N), it is not surprising that the Flory theory does not converge at $\rho=0$ or any other limits. Rather, as we have previously noted, the only surprise is how well the Flory theory performs in the high density limit, a result which is no doubt due to a fortuitous cancellation of errors that are inherent to the approximations used.

At low and medium densities $\rho \in [0,0.6]$, the MBSP phase boundary is very close to that of the exact phase boundary, while at high ρ, it shifts to λ values lower than those of the exact boundary. The MBSP theory even predicts an entropy-driven phase transition (i.e., for $\lambda=0$) for the $N=30$ chain at a solvent density of $\rho=0.86$. By contrast, the PRISM-HNC and PRISM-PY phase boundaries diverge from the exact phase boundary immediately with increasing ρ. For almost the entire range of solvent density considered here ($\rho \in [0,0.9]$), the PRISM calculations employing these two solvation potentials overestimate the stability of the coil state with respect to the globule state of the polymer. For densities up to $\rho=0.4$, the two curves are very close, after which, they diverge with the PRISM-HNC predicting a stable globule state over an increasingly wider range of λ than the case for PRISM-PY. Indeed, the PRISM-HNC phase boundary comes close to predicting an entropic phase transition at the highest density considered here, i.e., $\rho=0.9$. Unlike the case for PRISM-HNC, PRISM-PY always overestimates the range of stability of the coil phase, which lies at higher λ values than those of the exact boundary for all solvent densities considered here.

As discussed in Sec. III E, one criterion that is often used to define the polymer collapse transition point (in contrast to the condition $\nu=\frac{1}{2}$ employed here) is $B_2=0$, where B_2 is the second virial coefficient of the polymer chain. Here, B_2 is defined according to relation (44), but with the pair potential $u(r)$ replaced with the total effective pair potential of Eq. (31). As mentioned earlier, Fig. 2 shows that the transition point predicted by the conditions $\nu=\frac{1}{2}$ and $B_2=0$ are close but not equal. Figure 6(b) shows the resulting phase boundaries calculated using each of the two criteria for PRISM-HNC and PRISM-PY. As is clearly evident, the $\nu=\frac{1}{2}$ and $B_2=0$ phase boundaries follow the same general trends and are even quantitatively fairly close. This discrepancy is expected to diminish with increasing chain length and vanish in the limit $N\to\infty$. Note that the condition $B_2=0$ is useful only for theories employing polymer models with solvent-induced *pair* potentials between monomers. Consequently, it cannot be used with the MBSP potential.

As PRISM theory is essentially a distribution function based theory, it is instructive to compare the calculated and exact distribution functions. As described in Sec. III, the key distribution function calculated in the PRISM equations is $g_{\mathrm{ms}}(r)$. Figure 7(a) shows $g_{\mathrm{ms}}(r)$ calculated using both PRISM-HNC and PRISM-PY overlaid on that measured in the explicit-solvent DMD simulations. At first glance, there appears to be little difference between either theoretical prediction and the exact result. A clearer picture is provided by the inset of the figure, which shows plots of $\Delta g_{\mathrm{ms}}(r) \equiv g_{\mathrm{ms}}^{\mathrm{PRISM}}(r) - g_{\mathrm{ms}}^{\mathrm{DMD}}(r)$ versus r. We see that PRISM-HNC generally provides a more accurate prediction of the pair distribution function than PRISM-PY. In spite of this seemingly small difference between the two theories, it does nevertheless have a significant effect on the corresponding solvation pair potentials and thus on the predicted conformational behavior of the polymer. Figure 7(b) shows the HNC-type and PY-type solvation pair potentials, which have been calculated from $g_{\mathrm{ms}}(r)$ using Eqs. (28) and (30), respectively. While the two potentials correspond very

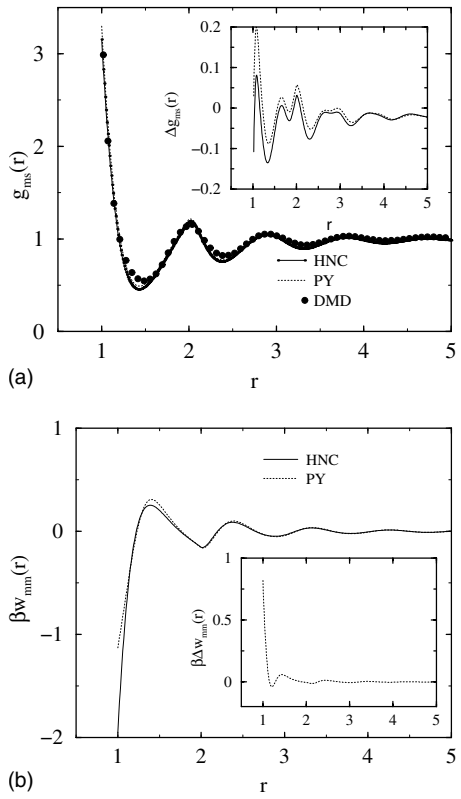

FIG. 7. (a) ms radial distribution function $g_{ms}(r)$ for model I for a polymer of length $N=30$ in a solvent at a density $\rho=0.9$ and a hydrophobicity parameter $\lambda=0.0$. The solid line is the prediction from a MC/PRISM calculation using the HNC-type solvation potential of Eq. (28), and the filled circles are the results from the explicit-solvent DMD simulation from Ref. 40. The inset shows the difference between the two, $\Delta g_{ms}(r) \equiv g_{ms}^{PRISM}(r) - g_{ms}^{DMD}(r)$. (b) Corresponding HNC-type and PY-type solvation potentials $\beta w_{mm}(r)$. The inset shows the difference between the two solvation potentials, $\beta \Delta w_{mm}(r) = \beta(w_{mm}^{HNC} - w_{mm}^{PY}(r))$.

closely over most distances, they diverge significantly at the mm contact point $r=\sigma$. As is more clearly shown in the inset, which plots the difference between the two solvation pair potentials, the difference in the depth of the attractive well at this point is about $0.8k_BT$. It is this greater effective potential well depth for the HNC-type potential compared to that for the PY-type potential, which leads to PRISM-HNC predicting a much wider range of stability for the globule relative to that predicted by PRISM-PY. Note that the difference between the HNC-type and PY-type potentials observed here is consistent with that observed in other studies.[18,25] While the results presented in Fig. 7 correspond to the athermal (i.e., $\lambda=0$) limit for model I, similar trends were observed over the full range of λ, i.e., $\lambda \in [0,1]$.

Thus far, we have presented results for model I with a mm range of attraction of $f=1.5$ (i.e., an attractive square well of width 0.5). Let us now examine how the predictions vary with f. Figure 8 shows a phase boundary in the ρ-f plane for model I system at density $\rho=0.9$, the highest density considered both in this study and in the DMD simulation study of Ref. 40. The behavior of the predicted results is consistent over the range $f \in [1.1,2]$; that is, PRISM-HNC tends to overpredict, while PRISM-PY tends to underpredict the range of stability of the globule state. Finally, we note once again that the simple Flory-type theory described in

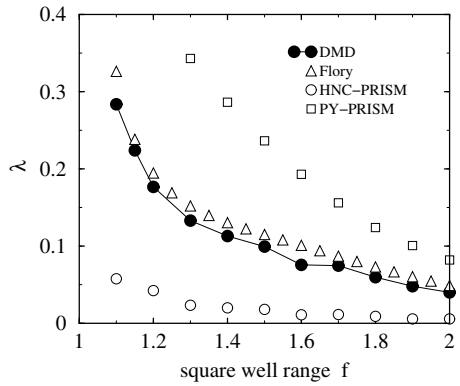

FIG. 8. Coil-globule phase boundaries in the λ-f plane for model I with a polymer of length $N=30$ in a solvent of density $\rho=0.9$ and at a temperature of $T=1.0$. f is the range of the mm potential square well, as defined in Eq. (1). Phase boundaries calculated using explicit-solvent DMD simulations and from a Flory-type mean-field theory are taken from Ref. 40.

Ref. 40 provides, by far, the most accurate estimate of the transition point at high density, although this is almost certainly a consequence of a fortuitous cancellation of errors inherent to the approximations made in the theory.

B. Model II

We now present the key results for the second polymer/solvent model considered in this study. In contrast to the extensive analysis and discussion of the results for model I in the previous section, only a comparison of theoretical and explicit-solvent coil-globule phase boundaries will be presented. In addition, recall that the MBSP potential was derived from SPT using a hard-sphere solvent. Since model II uses a solvent with attractions between solvent pairs, the MBSP approach of Ref. 26 is not appropriate to use with this model. Although the theory could probably be modified for use with arbitrary solvents, this is beyond the scope of the present study. Consequently, only theoretical predictions using PRISM theory are presented.

Figure 9 shows the calculated coil-globule phase bound-

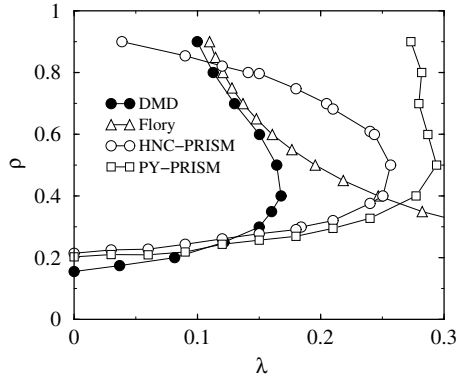

FIG. 9. Coil-globule phase boundaries for model II with a polymer of length $N=30$, a range of attraction of $f=1.5$, and at a temperature of $T=2.0$. The coil and globule regions are to the left and to the right of the phase boundaries, respectively. Theoretical predictions are shown for the PRISM theory with the HNC-type potential of Eq. (28) (open circles) and with the PY-type potential of Eq. (30) (open squares). In addition, explicit-solvent DMD simulation data (filled circles) and theoretical predictions from a Flory-type mean-field theory (open triangles), both taken from Ref. 40, are also shown.

aries for model II polymer/solvent system with a polymer of length $N=30$ and with a pair potential square-well range of $f=1.5$. The temperature of $T=2.0$ was chosen to be above the critical temperature of the solvent. The PRISM-HNC and PRISM-PY boundaries are overlaid on that calculated from the explicit-solvent simulations of Ref. 40. Note that the phase behavior is fundamentally different than that of model I. In this case, we did *not* observe a monotonic increase in the stability of the globule phase relative to that of the coil. Instead, at sufficiently low solvent density, the globule state is stable for the *entire* range of λ. This occurs because, at the temperature employed here ($T=2.0$), the mm attractions are sufficiently strong to favor a collapsed state of an isolated polymer. On the other hand, the solvent particles are also attracted to the monomers, and this attraction scales with $1-\lambda$. Consequently, for sufficiently *small* λ, the ms attractions cause a screening of the mm attractions. The degree of this screening increases with increasing solvent density, and the chain eventually undergoes a transition from the globule to the coil state. This screening effect has also been observed for other similar model systems.[30,31,37,38,53] As the solvent density increases further, however, the entropic effects of the solvent become increasingly important and lead to a slight compression of the chain. The combined effects result in the re-entrant behavior shown in Fig. 9.

Figure 9 also shows that both PRISM-HNC and PRISM-PY predict the coil state to be unfavorable at low solvent densities for any value of λ, consistent with the explicit-solvent simulation results. In all cases, the minimum density at which the coil is stable occurs at $\lambda=0$, i.e., for maximum ms attraction, where the screening effect is expected to be the most pronounced. At this point the transition occurs at a slightly higher density for each theoretical prediction ($\rho=0.215$ and 0.203 for PRISM-HNC and PRISM-PY, respectively) than that for the simulation result ($\rho=0.155$). Generally, the PRISM-HNC phase boundary follows the same qualitative trends as that of the exact phase boundary: above the lower-limit density, PRISM-HNC predicts a coil state whose λ range first increases, then decreases with increasing density, thus leading to the same re-entrant behavior present for the exact coil-globule transition boundary. However, the quantitative agreement is rather poor: The coil state has a range of stability that is far too wide at intermediate solvent density ($\rho\approx0.5$) and a range that is far too narrow at high density ($\rho=0.9$). It is noteworthy that the PRISM-HNC phase boundary crosses the simulation boundary at approximately the same density as was the case for model I ($\rho\approx0.8$). The origin of this discrepancy is the same for model II as it was for model I: The solvent-mediated effective mm attraction is too small for intermediate ρ and too large for high ρ. The PRISM-PY curve is coincident with the PRISM-HNC curve at lower solvent density, but diverges at higher ρ. For $\rho\in[0.5,0.9]$, the range of stability of the coil state by PRISM-PY is overpredicted by a factor ranging from 2 to 2.75. The behavior of the PRISM-PY curve at intermediate and high densities for model II (i.e., overestimation of the range of stability of coil state) is qualitatively consistent with the results of model I. Thus, independent of the model employed, the PY solvation potential underestimates the solvation-mediated mm attraction over this density range. The HNC and PY solvation potentials for model II are comparable to those shown in Fig. 7(b) for model I (data not shown).

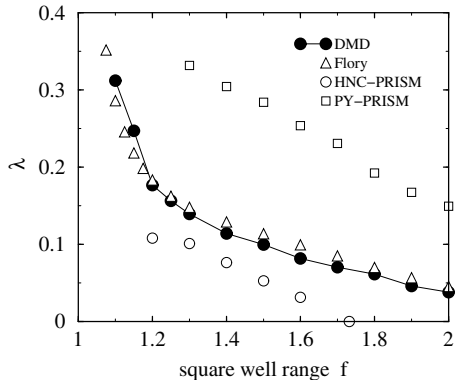

FIG. 10. Coil-globule phase boundaries in the λ-f plane for model II, with a polymer of length $N=30$ in a solvent of density $\rho=0.9$ and at a temperature of $T=2.0$. f is the range of the mm potential square well, as defined in Eq. (2). Phase boundaries calculated using explicit-solvent DMD simulations and from a Flory-type mean-field theory are taken from Ref. 40.

The phase boundaries shown in Fig. 9 were calculated for a system with a square-well attraction range of $f=1.5$. As in the case of model I, we have also investigated the effect of variation in f on the coil-globule transition point at high solvent density. Figure 10 shows calculated coil-globule phase boundaries in the λ-f plane at $\rho=0.9$ for a model II polymer/solvent system. The results are very similar to those for model I system in Fig. 8. Again, we observe that PRISM-HNC consistently overestimates the compressive effect of the solvent on the chain at high density and so underestimates the range of stability of the coil state for the full spectrum of attractive potential ranges considered here, $f\in[1.1,2.0]$. In fact, PRISM-HNC predicts that the globule is stable for all energy mismatch λ values for square-well ranges greater than 1.73 (i.e., for square-well widths greater than 0.73). On the other hand, PRISM-PY consistently overestimates the range of stability of the coil. We conclude that overestimation of the effective mm attractions by the HNC solvation potential and underestimation of these attractions by the PY solvation potential at high ρ is a generic result that is independent of the range of true attraction between interaction sites and is independent of the polymer/solvent model employed.

V. CONCLUSIONS

In this study, we have used two different theoretical approaches to study the coil-globule transition of a polymer in a solvent. The first approach uses the PRISM theory together with a solvation potential in a self-consistent MC simulation of a single-polymer chain to calculate the conformational state of the polymer. Two commonly used solvation potentials were considered: One derived using the HNC closure relation and another derived using the PY closure relation. Each of the solvation potentials employed with the PRISM calculations are pairwise additive. The second theoretical approach used a MC simulation of a single chain with a multi-

body solvation potential that was introduced over a decade ago by Grayce.[26] This solvation potential, which is derived using SPT, depends on the overall size and shape of the molecule and is *not* pairwise additive. The theoretical predictions were compared to explicit-solvent DMD simulations of two simple polymer/solvent model systems. The purpose of the study was to assess the accuracy of each of the theories in describing the conformational properties of the polymer over a range of solvent conditions and in locating the coil-globule transition point.

The predictions of the conformational properties of the polymer chain using the PRISM theory were highly dependent on the choice of solvation potential. Neither the HNC-type nor the PY-type solvation potentials were quantitatively accurate in predicting the location of the coil-globule transition or the variation in the polymer size with the degree of hydrophobicity. Calculations using the HNC potential tended to overestimate the solvent-mediated attraction between monomers at high solvent densities and underestimate this attraction at intermediate and low solvent densities. The predictions obtained from calculations using the PY potential tended to underestimate this attraction for all solvent densities. These discrepancies between theory and simulation appear to worsen with increasing chain length. Our results are consistent with results from previous studies employing the PRISM theory to study polymer conformational behavior in good solvent conditions at high solvent densities. However, our calculations have expanded the range of solvent conditions and densities over which these trends have been observed.

The accuracy with which the coil-globule phase boundaries and pair distribution functions are predicted by the PRISM/MC hybrid method clearly depends on the validity of the various approximations that were described in Sec. III. These approximations include those that were used to construct the solvation potentials used in the MC simulations as well as those intrinsic to the PRISM method itself. Approximations in the former category are (1) the assumption of pairwise additivity of the solvation potentials [cf. Eq. (20)], (2) the use of a *single* solvation pair potential, $w_{\mathrm{mm}}(r)$, to describe interactions between *any* pair of monomers [cf. Eq. (21)], (3) the decoupling of mm correlations implicit in Eq. (23), and (4) the closure relation used to solve the Ornstein–Zernicke equation in the derivation of $w_{\mathrm{mm}}(r)$. As described in Sec. I, recent work by Taylor demonstrates that a pairwise-additive solvation potential can yield quantitatively precise results in *good* solvent conditions for polymers of lengths up to $N=50$. Thus, assumption (1) is not necessarily a poor one, though it remains to be seen whether it can retain its validity over a wider range of solvent conditions and chain lengths. It is also worth noting that Taylor's method employed a *set* of pair potentials, as opposed to a single pair potential of assumption (2). To our knowledge, there is no solvation potential satisfying both conditions (1) and (2) that accurately predicts the conformational properties of polymers in solution. In the present study, the large difference between the PRISM-HNC and PRISM-PY predictions demonstrate that the self-consistent PRISM/MC approach is highly sensitive to condition (4). This has been noted in earlier PRISM studies, and it is not surprising to find it true in the context of the polymer collapse transition. Alternative forms for solvation potentials of the type considered here could also be investigated. For example, the authors of Ref. 25 investigated the Martinov–Sarkisov solvation potential in addition to the HNC and PY potentials. Preliminary calculations in the present study found that this potential yielded results comparable to those of the PY potential, and so we decided not to pursue this approach. Mendez *et al.* used the HNC potential with an *ad hoc* scaling factor to correct the overestimation of the solvent-mediated attraction between monomers at high solvent density.[22,23] Note, however, that this correction factor is expected to vary with solvent density and that it can only be determined if the explicit-solvent simulation results are already available. Consequently, it is not a particularly useful approach for the purpose of *predicting* the location of the coil-globule transition. Finally, as stated above, in addition to the approximations used to construct an appropriate solvation potential, there are others inherent to the PRISM method itself, including the closure relations used to solve the PRISM equation, the equivalence of sites approximation [i.e., the use of a single $g_{\mathrm{MS}}(r)$ function to describe ms correlations], as well as the approximations inherent in the RISM theory, upon which PRISM is based. If a solvation potential could be discovered (pairwise additive or not) that yields quantitatively precise predictions of the conformational behavior of the polymer, then the validity of some of these other approximations could be properly examined.

The multibody solvation potential introduced by Grayce in 1997 provides a convenient alternative to the pairwise-additive potentials typically employed in PRISM studies of polymer/solvent systems. The results from that study strongly suggested that it would yield considerably more accurate predictions of polymer conformational behavior compared, for example, to the HNC and PY potentials.[26] We were therefore somewhat surprised to find that the theoretical predictions were not accurate over the complete range of conditions considered in this study. At low and intermediate densities the predictions of the coil-globule transition point, as well as the polymer size over a range of hydrophobicity, were very accurate for model I system. However, at higher densities the predictions were very poor for a polymer chain of length $N \geqslant 20$, even in the athermal limit of $\lambda=0$. It should be noted that Grayce only tested the potential for N-mers of length $N=3$ and $N=10$ for an athermal system. (In addition, Grayce employed a polymer model with fixed-bond length, in contrast to our model, which uses a polymer with variable bond length, though that is unlikely to make a substantial difference.) Worse still, the discrepancy between the MBSP theoretical prediction and the exact results at high density appear to grow with increasing chain length. We conclude that the MBSP solvation potential of Grayce, at least in its original form, does not provide an appreciably better alternative for studying single-chain polymer collapse at liquidlike solvent densities to the PRISM/MC hybrid method with conventional pairwise-additive solvation potentials.

ACKNOWLEDGMENTS

This work has been supported by the National Research Council of Canada (NSERC) and by the Canadian Foundation for Innovation (CFI). We are grateful to the Advanced Computational Research Laboratory (ACRL) at the University of New Brunswick and to WestGrid for use of their computational facilities.

[1] I. Nishio, S.-T. Sun, G. Swislow, and T. Tanaka, Nature (London) **281**, 208 (1979).
[2] G. Swislow, S.-T. Sun, I. Nishio, and T. Tanaka, Phys. Rev. Lett. **44**, 796 (1980).
[3] B. M. Baysal and F. E. Karasz, Macromol. Theory Simul. **12**, 627 (2003).
[4] H. H. Gan and B. C. Eu, J. Chem. Phys. **109**, 2011 (1998).
[5] M. P. Taylor and J. E. G. Lipson, J. Chem. Phys. **104**, 4835 (1996).
[6] M. P. Taylor, J. Chem. Phys. **121**, 10757 (2004).
[7] M. P. Taylor and G. M. Peterson, J. Chem. Phys. **127**, 184901 (2007).
[8] M. P. Taylor and S. Ichida, J. Polym. Sci., Part B: Polym. Phys. **45**, 3319 (2007).
[9] T. Sumi and H. Sekino, J. Chem. Phys. **122**, 194910 (2005).
[10] A. Milchev, W. Paul, and K. Binder, J. Chem. Phys. **99**, 4786 (1993).
[11] K. S. Schweizer and J. G. Curro, Phys. Rev. Lett. **58**, 246 (1987).
[12] K. S. Schweizer and J. G. Curro, Adv. Polym. Sci. **116**, 321 (1994).
[13] K. S. Schweizer and J. G. Curro, Adv. Chem. Phys. **98**, 1 (1997).
[14] D. Chandler and H. C. Andersen, J. Chem. Phys. **57**, 1930 (1972).
[15] D. Chandler and H. C. Andersen, in *Studies in Statistical Mechanics VIII*, edited by E. W. Montroll (North-Holland, Amsterdam, 1982).
[16] D. Chandler, Y. Singh, and D. M. Richardson, J. Chem. Phys. **81**, 1975 (1984).
[17] C. J. Grayce and K. S. Schweizer, J. Chem. Phys. **100**, 6846 (1994).
[18] C. J. Grayce, A. Yethiraj, and K. S. Schweizer, J. Chem. Phys. **100**, 6857 (1994).
[19] P. G. Khalatur and A. R. Khokhlov, Mol. Phys. **93**, 555 (1998).
[20] P. G. Khalatur, L. V. Zherenkova, and A. R. Khokhlov, Eur. Phys. J. B **5**, 881 (1998).
[21] V. V. Vasilevskaya, P. G. Khalatur, and A. R. Khokhlov, J. Chem. Phys. **109**, 5108 (1998).
[22] S. Mendez, J. G. Curro, M. Pütz, D. Bedrov, and G. D. Smith, J. Chem. Phys. **115**, 5669 (2001).
[23] S. Mendez and J. G. Curro, J. Phys. Chem. **37**, 1980 (2004).
[24] L. Livadaru and A. Kovalenko, J. Phys. Chem. **121**, 4449 (2004).
[25] L. Livadaru and A. Kovalenko, J. Phys. Chem. **109**, 10631 (2005).
[26] C. J. Grayce, J. Chem. Phys. **106**, 5171 (1997).
[27] M. Dijkstra, D. Frenkel, and J.-P. Hansen, J. Chem. Phys. **101**, 3179 (1994).
[28] M. Dijkstra and D. Frenkel, Phys. Rev. Lett. **72**, 298 (1994).
[29] G. Luna-Bárcenas, G. E. Bennett, I. C. Sanchez, and K. P. Johnston, J. Chem. Phys. **104**, 9971 (1996).
[30] G. Luna-Bárcenas, J. C. Meredith, I. C. Sanchez, K. P. Johnston, D. G. Gromov, and J. J. de Pablo, J. Chem. Phys. **107**, 10782 (1997).
[31] G. Luna-Bárcenas, D. G. Gromov, J. C. Meredith, I. C. Sanchez, J. J. de Pablo, and K. P. Johnston, Chem. Phys. Lett. **278**, 302 (1997).
[32] J. K. C. Suen, F. A. Escobedo, and J. J. de Pablo, J. Chem. Phys. **106**, 1288 (1997).
[33] J. M. Polson, Phys. Rev. E **60**, 3429 (1999).
[34] J. M. Polson and M. J. Zuckermann, J. Chem. Phys. **113**, 1283 (2000).
[35] R. Chang and A. Yethiraj, J. Chem. Phys. **114**, 7688 (2001).
[36] J. M. Polson and M. J. Zuckermann, J. Chem. Phys. **116**, 7244 (2002).
[37] M. Lísal and I. Nezbeda, J. Chem. Phys. **119**, 4026 (2003).
[38] M. Lísal and I. Nezbeda, Fluid Phase Equilib. **222–223**, 247 (2004).
[39] J. M. Polson and N. E. Moore, J. Chem. Phys. **122**, 024905 (2005).
[40] S. B. Opps, J. M. Polson, and N. Abou Risk, J. Chem. Phys. **125**, 194904 (2006).
[41] F. A. Escobedo and J. J. de Pablo, Mol. Phys. **89**, 1733 (1996).
[42] J.-P. Hansen and I. R. MacDonald, *The Theory of Simple Liquids*, 3rd ed. (Academic, Amsterdam, 2006), pp. 95–97.
[43] K. S. Schweizer and A. Yethiraj, J. Chem. Phys. **98**, 9053 (1993).
[44] K. S. Schweizer and A. Yethiraj, J. Chem. Phys. **98**, 9080 (1993).
[45] D. Chandler and L. R. Pratt, J. Chem. Phys. **65**, 2925 (1976).
[46] Y. Singh, J. Phys. A **20**, 3949 (1987).
[47] A. A. Broyles, J. Phys. Chem. **33**, 456 (1960).
[48] J.-L. Barrat and J.-P. Hansen, *Basic Concepts for Simple and Complex Liquids* (Cambridge University Press, Cambridge, 2003).
[49] J. Busa, J. Dzurina, E. Hayryan, S. Hayryan, C. K. Hu, J. Plavka, I. Pokorny, J. Skrivanek, and M. C. Wu, Comput. Phys. Commun. **165**, 59 (2005).
[50] H.-P. Hsu, W. Nadler, and P. Grassberger, Macromolecules **37**, 4658 (2004).
[51] T. Prellberg, J. Phys. A **34**, L599 (2001).
[52] P. Belohorec and B. G. Nickel, University of Guelph Report 1997 (unpublished).
[53] M. P. Taylor, J. Chem. Phys. **123**, 167101 (2005).